X-ray attenuation properties of commonly employed solid oxide fuel cell materials

2017 J. Phys.: Conf. Ser. 849 012017

(http://iopscience.iop.org/1742-6596/849/1/012017)

IOP Conf. Series: Journal of Physics: Conf. Series **849** (2017) 012017 doi:10.1088/1742-6596/849/1/012017

X-ray attenuation properties of commonly employed solid oxide fuel cell materials

T M M Heenan, D J L Brett and P R Shearing*

Electrochemical Innovation Lab, Department of Chemical Engineering, UCL, London, UK, WC1E 7JE

*E-mail: p.shearing@ucl.ac.uk

Abstract. X-ray nano CT has been vastly applied to study the microstructure of solid oxide fuel cell (SOFC) electrodes. One widely accepted indicator of electrochemical performance is the triple phase boundary (TPB): a location where the three materials responsible for ionic, electronic and gas-phase reactant transport are in contact. X-ray absorption tomography has been used extensively in the characterisation of these TPBs, utilising the different attenuation properties of the constituent materials. Here we present a quantitative comparison of the attenuation properties for elements commonly employed in solid oxide fuel cell materials.

1. Introduction

Offering high efficiencies and fuel versatility, solid oxide fuel cells (SOFCs) offer great promise in the future of energy conversion technology. In their most simple form, a SOFC is comprised of two electrically conducting electrodes separated by an electrically insulating, ionically conducting electrolyte. Reduction and oxidation reactions occur at the cathode and anode electrodes respectively, with ion transport occurring through the electrolyte layer. It is widely accepted that the reaction sites in composite electrodes are located at the boundary of the three transport phases (electronic, ionic and reactant transport), the so-called triple phase boundaries (TPBs). Characterisation methods including X-ray nano CT and FIB-SEM slice and view allow for the calculation of TPB densities [1].

Commonly employed anode materials include Ni cermets, with a ceramic such as yttria-stabilised zirconia (YSZ) or gadolinium-doped ceria (GDC), whereas cathodes commonly contain a lanthanum strontium compound containing either manganite (LSM) or cobalt ferrite (LSFC) which can also be coupled with the YSZ or GDC ceramics [1 – 3].

Presented here, is an analysis of the key X-ray properties which dictate the reliability of image segmentation of SOFC materials via X-ray nano CT techniques. This includes consideration of the influence of dopant concentrations on the attenuation of composite metal-ceramic cermets and the location of the optimum imaging energies to achieve three-phase segmentation for such cermet materials.

2. Properties of solid oxide fuel cell materials: elements, compounds and cermets.

X-ray absorption tomography has been widely employed in the characterization of SOFC microstructures [1]. Triple phase boundaries (TPBs) within SOFC electrodes have become a widely accepted metric as an indicator of electrochemical performance. In order to locate such boundaries, multi-phase segmentation is required, which can only be achieved with knowledge of several attenuation characteristics of the constituent materials. One method to achieve such segmentation is X-ray absorption spectroscopy (XAS) imaging which has been employed to achieve solid-solid segmentation (typically metal and ceramic) [4, 5].

Nomenclature

L	Thickness	μm
I	X-ray intensity	counts
w	Mass Fraction	no-units
AC	Attenuation Coefficient	no-units
x	Dopant concentration	mol %
Greek Letters		
μ	Linear AC	μm^{-1}
μ_m	Mass AC	$\mu m^2 g^{-1}$
λ	Attenuation Length	μm
ρ_m	Mass Density	$g \mu m^{-3}$
η	Contrast Coefficient	no-units
Subscripts		
i	Material i	
k	Compound k	
0	Incident	

Three metrics of the ability to visualise the difference in attenuation of the constituent materials, and thus the ability for image segmentation, are the mass attenuation coefficient, μ_m, linear attenuation coefficient, μ, and the attenuation length, λ. These three properties can be derived from the exponential decay of X-ray intensity when passing through a material described by Equation 1 for material i [5].

Comprehensive lists of the mass attenuation coefficients and attenuation lengths are presented elsewhere [6, 7, 8] and the linear attenuation coefficient can be calculated from the mass attenuation coefficient using Equation 2.

The attenuation length is defined as the distance, L, perpendicular to the material surface through which the X-ray intensity, I, has decayed to 1/e that of the intensity at the material surface, I_o. Inserting these conditions into Equation 1 results in the relationship between attenuation length and the linear attenuation coefficient displayed in Equation 3.

$$\frac{I}{I_0} = \exp\left[-\mu_{m_i} L \rho_{m_i}\right] \tag{1}$$

$$\mu_i = \mu_{m_i} \rho_{m_i} \tag{2}$$

$$\lambda_i = \frac{1}{\mu_i} \tag{3}$$

Although elemental data for the attenuation properties of solid oxide fuel cells is readily available, many materials contain several elements in order to achieve the desired thermo-mechanical and electrochemical properties [9]. Examples being yttria – stabilised zirconia (YSZ), gadolinium – doped ceria (GDC), lanthanum strontium manganite (LSM) and lanthanum strontium cobalt ferrite (LSCF). Equation 4 can be employed in order to obtain the mass attenuation coefficients for compound materials via summation of the i constituent elements weighted according to their respective mass fractions (w_i) in compound k [7].

$$\mu_{m_k} = \sum_i w_i \left(\frac{\mu_i}{\rho_{m_i}}\right) \tag{4}$$

Common laboratory X-ray sources using copper, Cu, or chromium, Cr, for X-ray generation provide peak energies at 8.0 and 5.4 keV respectively. Hence, when inspecting the variation of attenuation properties using Equation 4 across the commonly employed range of dopant concentrations used during xYSZ fabrication ($3 \leq x \leq 8$ mol% yttria addition to zirconia) a fixed energy of 5.4 keV was chosen [10]. It was found that the compound mass attenuation coefficient for xYSZ deviated insignificant amounts through the entire dopant range; the xYSZ mass attenuation coefficient reduced by less than 0.5 $cm^2 g^{-1}$ from 3 to 8 mol %. The elemental contribution to attenuation properties was then inspected by considering the difference in mass attenuation coefficient between zirconium, the primary element within xYSZ, and Ni; $\mu_{m_{Zr}}$ is ca. 166% larger than $\mu_{m_{Ni}}$ at 5.4 keV. Concluding that at 5.4 keV the ability to obtain triple phase segmentation is greatly dependent upon the elemental contribution whereas doping level has negligible effect for xYSZ.

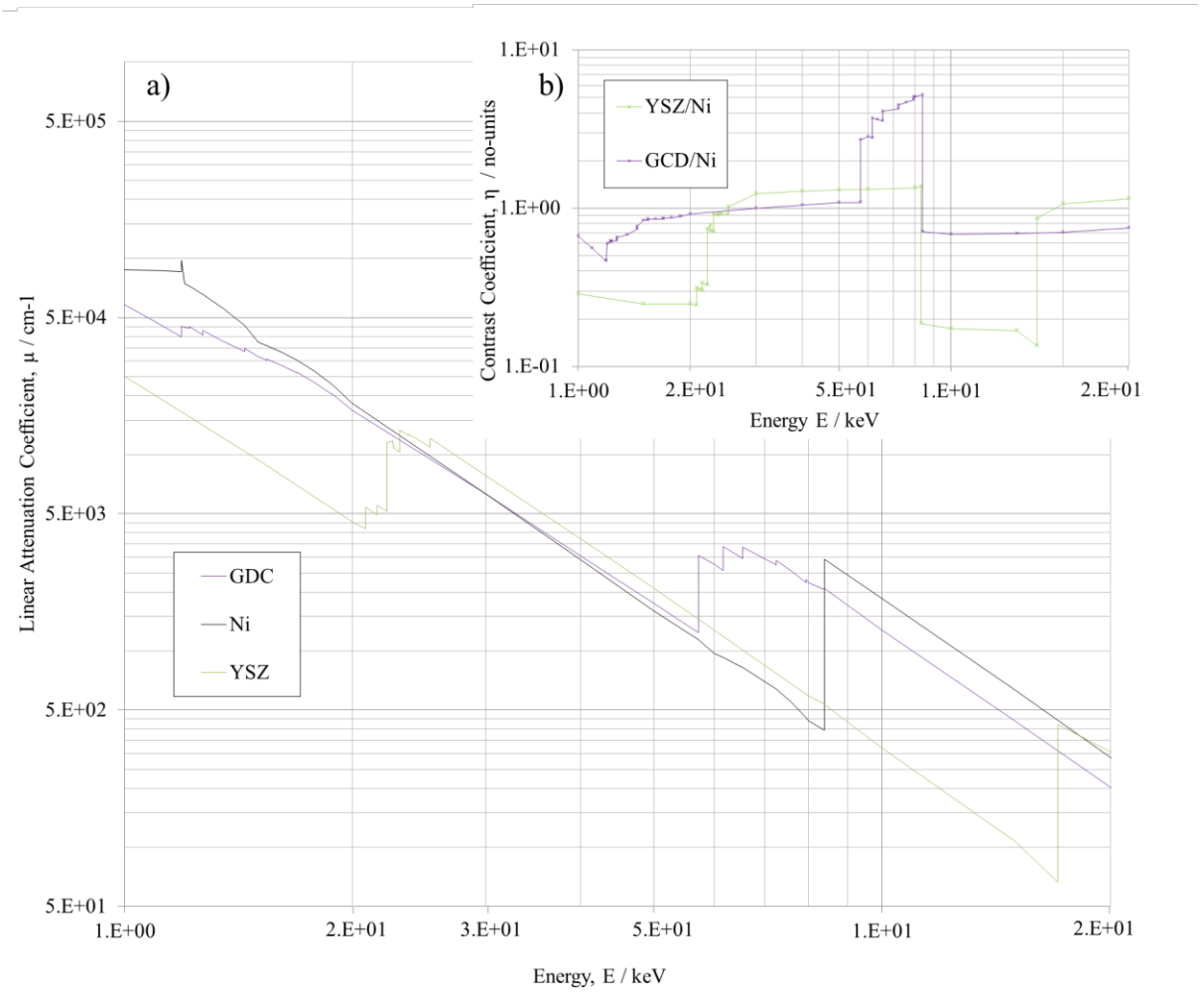

Figure 1. Locating the optimal segmentation energies between 1 and 20 keV using XAS techniques for Ni-8YSZ and Ni-3GDC electrodes: a) the linear attenuation coefficients for commonly employed solid oxide fuel cell materials: pure nickel, zirconia stabilised with an addition of 8 mol % yttrium oxide and ceria doped with 3% gadolinium, and b) the contrast quality through the same energy range quantified by the contrast coefficients (the ratio of linear attenuation coefficients) for the cermet materials.

Monochromatic X-ray tomography is conducted at a fixed energy chosen specific to the experiment in order to optimise segmentation of the microstructure. Therefore, with use of Equation 4 and the elemental data for nickel, yttrium, zirconium, gadolinium, cerium and oxygen from [7], Figure 1 a. was produced displaying the variation of linear attenuation coefficient for Ni, 8-YSZ and 3-GDC with X-ray energies between 2 and 30 keV. The linear attenuation coefficients for 8YSZ and 3GDC were then compared to the linear attenuation coefficient for Ni using Equation 5, by defining a variable which quantifies contrast: the contrast coefficient, η.

$$\eta = \frac{\mu_{Ceramic}}{\mu_{Ni}} \tag{5}$$

Segmentation of the ceramic and metal is optimal at contrast coefficients most distant from unity i.e. optimal segmentation is achieved when $\eta \gg 1 \; or \; \eta \ll 1$. The contrast coefficients for both Ni-8YSZ and Ni-3GDC are displayed in Figure 1 b. From the figure it is evident that, given a choice

of x-ray energies such as at a synchrotron, XAS conducted at energies just below the Ni K-edge will provide greatest segmentation possibility for the Ni-3GDC cermet while XAS conducted just above the Ni K-edge will produce the best results for the Ni-8YSZ cermet, 8 and 9 keV respectively. It is also seen that, due to the highly attenuating properties of 3GDC below the Ni K-edge, the contrast coefficient for Ni-3GDC is potentially far greater than Ni-8YSZ if the correct energy is chosen. For the commonly used laboratory X-ray sources Cr and Cu the contrast coefficients for Ni-3GDC and Ni-8YSZ is quantified and presented in Table 1.

Table 1. Contrast coefficients for two commonly employed lab-based X-ray sources Cr and Cu for two cermet materials Ni-3GDC and Ni-8YSZ.

X-ray source	**Peak Energy / keV**	$\eta_{Ni-3GDC}$ **/ no-units**	$\eta_{Ni-8YSZ}$**/ no-units**
Chromium, Cr	5.4	1.09	1.31
Copper, Cu	8.0	5.08	1.34

3. Conclusion

In order to achieve TPB data for common SOFC materials from X-ray techniques, the different attenuation properties of the constituent materials must be understood.

Presented here, are the attenuation properties, namely the mass attenuation coefficient, linear attenuation coefficient and attenuation length, for commonly employed solid oxide fuel cell materials. The linear attenuation coefficient for two ceramic compounds, YSZ and GDC is calculated for a large range of energies (2 – 30 keV) and the theoretical phase contrast quality is quantified via definition of a contrast coefficient for both the Ni-8YSZ and Ni-GDC cermets. It is concluded that optimal contrast can be obtained at ca. 8 keV for Ni-3GDC and ca. 9 keV for Ni-8YSZ, i.e. just below and above the Ni K-edge for Ni-GDC and Ni-YSZ respectively. Furthermore, given the choice of either chromium or copper for a fixed energy lab source, copper would present the greatest solid-phase contrast for both Ni-YSZ and Ni-GDC.

Improved application of X-ray attenuation properties for electrochemical devices such as solid oxide fuel cells will aid in the understanding of cell degradation thus lead to improved life times via reduced performance losses leading to greater competitiveness in the energy market.

References

[1] Shearing P R, Brett D J L and Brandon N P, 2013, *International Materials Reviews*, **55**.6, 347 – 63.
[2] Chunwen S, Hui R, and Roller J, 2009, *J Solid State Electrochem*, **14**.7, 1125 – 44.
[3] Zhu W Z, and Deevi S C, 2003, *Materials Science and Engineering: A*, **362**.1, 228 – 9.
[4] Rehr J J and Albers R C, 2000, *Reviews of modern physics*, **72**.3, 621.
[5] Shearing P R, Gleb J, Yi J, Lee W K, Drakopolous M and Brandon N P, 2010, *Electrochemistry Communications*, **12**.8, 1021-1024.
[6] Centre for X-ray Optics, *CXRO, 13/09/2016*, http://henke.lbl.gov/optical_constants/.
[7] Hubbell J H and Sheltzer S M, 12/09/2016, *National Institute of Standard and Technology, NIST*, http://physics.nist.gov/PhysRefData/XrayMassCoef/chap2.html.
[8] Henke B L, Gullikson E M, and Davis J C, 1993, X-ray interactions: photoabsorption, scattering, transmission, and reflection at E=50-30000 eV, Z=1-92, *Atomic Data and Nuclear Data Tables*, **54**.2, 181-342.
[9] Hayashi H, Saitou T, Maruyama N, Indaba H, Kawamura K and Mori M, 2005, *Solid State Ionics*, **176**.5, 613-619.
[10] Zeiss Xradia 810 Ultra 'Nanoscale X-ray Imaging: Explore at the speed of science', 2016, *http://pages.microscopy.zeiss.com/rs/zeiss/images/EN_42_011_080_Product_810Ultra.pdf*.

Acknowledgments

The authors would like to acknowledge the EPSRC (EP/M014045/1), the Centre for Doctoral training in Fuel Cells and their Fuels and the Royal Academy for Engineering for financial support.